On Latent Palmprint Matching

Anil K. Jain and Meltem Demirkus*

Abstract

The evidential value of palmprints in law enforcement is clear from the following statistic: 25% of all crime scenes contain only latent palmprints [1] and 30% of the latents recovered from crime scenes are of palms [2]. In forensic applications, the palmprint image resolution is 500 pixels per inch (ppi) [5] and the matching is based on friction ridges, flexion creases and minutiae points. Palmprint recognition has recently become popular for person authentication in commercial applications (e.g., access control). But, these applications utilize low resolution ($\sim$ 100ppi) images to keep the sensor cost and processing requirements low. The feature extraction and matching techniques used in these low resolution systems cannot be adopted for forensic applications since they do not (i) address latent palmprint matching, and (ii) do not use friction ridge and minutiae information. We propose a palmprint matching system utilizing a variety of palmar features (friction ridges, minutiae, flexion creases and palmar texture) present in 500 ppi images. Our system is able to match either a full or partial/latent input image to a database of full palmprint images. Since there is no public domain 500 ppi palmprint database, our results are based on an in-house database of 100 unique palms with 10 impressions per palm. We are able to achieve a genuine matching accuracy of 98.9% at an FAR of 0.01% for full-to-full palmprint matching. In case

Department of Computer Science & Engineering, 3115 Engineering Building, Michigan State University, East Lansing, MI 48824. Emails: {jain,demirkus}@msu.edu

of partial-to-full palmprint matching, rank-1 retrieval accuracies of 95.6% and 82% are achieved for synthetic latent and pseudo-latent palmprint databases, respectively.

Index Terms

Latent palmprints, palmprint matching, 500 ppi palmar features, minutiae matcher, SIFT.

I. INTRODUCTION

A palmprint is a combination of two unique features, namely, the *palmar friction ridges* and the *palmar flexion creases* (see Figure 1). Palmar friction ridges are the corrugated skin patterns with sweat glands but no hair or oil glands. Discontinuities in the epidermal ridge patterns are called the palmar flexion creases. These are the firmer attachment areas to the basal (dermis) skin structure. Flexion creases appear before the formation of friction ridges during the embryonic skin development stage, and both of these features are immutable, permanent and unique to an individual [8].

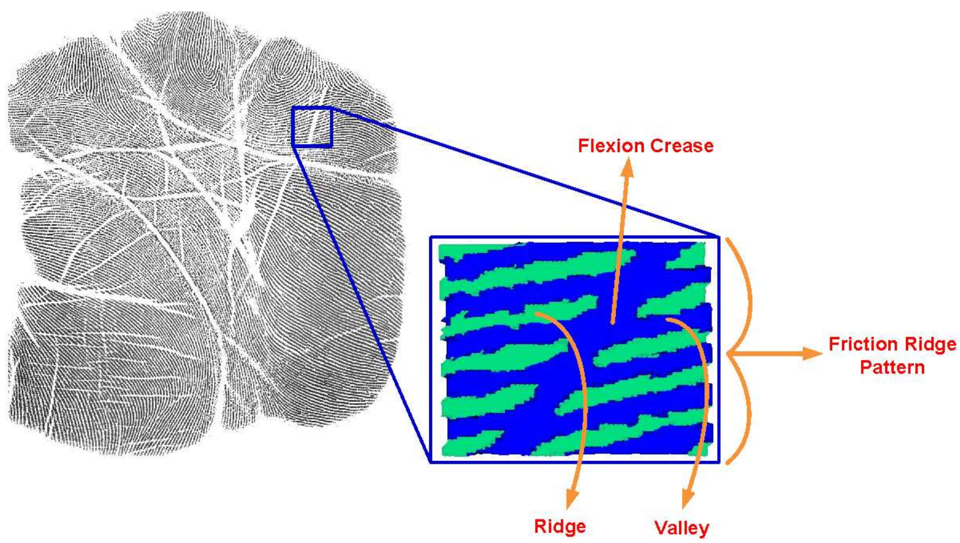

Fig. 1. A 500 ppi palmprint image with illustration of the palmar flexion creases and the palmar friction ridges.

The use of palmprint for person identification traces back to Chinese deeds of sale in the 16th century [12]. Later in 1684, Nehemiah Grew introduced one of the first scientific descriptions of dermatoglyphics, a description of the epidermal ridges and their arrangement on the hand. The first systematic capture of hand, finger and palm images for identification purposes was done by Sir William Herschel in 1858 [13]. Galton [7] discussed the basis of contemporary fingerprint science, and introduced the palmar ridges and creases. He suggested that the ridges on the finger tips, palms and soles are persistent and unique. Galton defined the peculiarities in the ridges as “minutiae”, introduced several different minutiae types, divided the palm into three regions and analyzed the correlation between the ridge flow and the major creases in each region. Cummins and Midlo [12] stated that the width of a palmar ridge is 18% larger compared to a finger. They also recognized the significance of the flexion creases, particularly palmar flexion creases, and founded the basis of the present flexion crease identification.

The study of embryology has shown that the development of friction ridge skin (FRS) is related to the formation of volar pads, that is, the temporary swelling of the mesenchymal tissue. Volar pads are formed on the palm, digits and finger during the early stages (from 6th to 8th week) of fetal development. Between the 10-th and 12-th week, the volar pads start to recede and the FRS begins to appear by taking the shape of the receding volar pads. The FRS pattern originates from the deeper dermis layer (inner layer) and eventually propagates to the epidermis layer (outer layer). Consequently, minor bruises and cuts to the epidermis layer do not alter the palmar friction ridge pattern. The friction ridges are composed of *ridge units* with a single pore on each of these units. The shape and size of the ridge units as well as the number of ridge units and their location along a ridge are random, and thus, serve to uniquely identify an individual.

To describe the location and direction of the palmar friction ridges and flexion creases with reference to the palm, several anatomical landmarks are defined: proximal, distal, radial and ulnar (see Figure 2 (a)). *Proximal* indicates the lower part of the palm close to the wrist region. *Distal* is the upper part of the palm in the direction of the fingers. *Radial* is the palmar region around the thumb consisting of the interdigital pad I and thenar eminence regions. *Ulnar* is the palmar region directly opposite to the radial which contains hypothenar eminence.

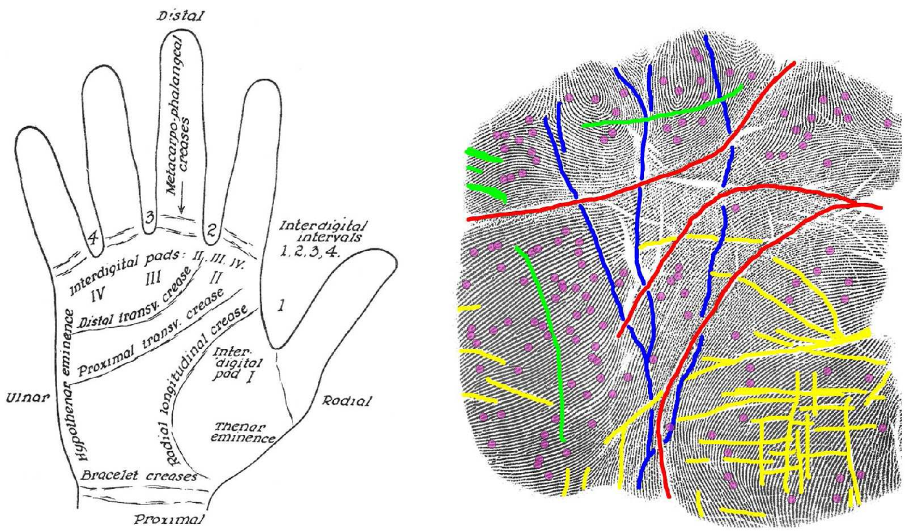

Fig. 2. Palmar physiology, a) Anatomical landmarks for the palm (adopted from [12]), b) Main groups of the palmar flexion creases: Major flexion creases (red), b) Minor flexion creases (green), c) Minor Finger Creases (blue), d) Secondary creases (yellow) and friction ridge details: minutiae (magenta).

There are three main groups of flexion creases appearing on the palm, namely *major flexion creases*, *minor flexion creases* and *secondary creases* [8]. Major flexion creases (Figure 2 (b)) are the most visible and the largest creases on the palm and form a consistent spatial arrangement. The three major types of flexion creases are: (1) distal transverse crease (the heart-line), (2) proximal transverse crease (the head-line) and (3) radial transverse crease (the life-line). Minor flexion creases have more variety in terms of their length, presence and importance compared to the major flexion creases (Figure 2 (b)). There are four types of minor flexion creases: (1) Longitudinal (finger crease), (2) accessory distal traverse crease, (3) E-lines, and (4) hypothenar crease. It should be noted that some palms do not have the accessory distal traverse crease. The third group of the flexion creases, called secondary creases, may be found anywhere on the palm (see Figure 2 (b)). While friction ridges are claimed to be unique to a palm, palmar flexion creases are also used in conjunction with friction ridges, if present, in the identification process.

While the use of fingerprint matching systems (AFIS) in the forensic community is pervasive [8], the development of Automated Palmprint Identification Systems (APIS) has lagged due to the limitations of live-scan technologies for palmprints, and large storage and computing capabilities needed for palmprints. The first reported use of palmprints in a criminal case occurred in a British court in 1931. The first Automated Palmprint Identification System is believed to have been built by a Hungarian company, RECOWARE in the early 1990s [3]. NEC's APIS became operational in 2001 and the first statewide palmprint database was established in Connecticut in 2004. In terms of the repository size, the Australian National Identification System comes first with about 5.6 million palmprint records [4] .

Over the past 10 years, a number of palmprint recognition systems have been developed for commercial applications (e.g., access control). These systems typically utilize low resolution (~ 100 ppi) images ([9]-[11]) and as such do not use the same set of features as used by forensic experts. As a result, the feature extraction and the matching algorithms developed for the low resolution palmprint matching cannot be used in forensics. Further, commercial palmprint matching systems do not deal with latent to full palmprint matching.

The rest of the paper is organized as follows: Section 2 gives the description of the full-to-full palmprint matching system while Section 3 describes the partial-to-full palmprint matching. Experimental results are provided in Section 4, with summary and conclusion presented in Section 5.

II. Full-to-full Palmprint Matching System

The block diagram of the proposed full-to-full palmprint matching system is shown in Figure 3. The system consists of three major components: (1) pre-processing, (2) feature extraction, and (3) minutiae matching. The preprocessing phase segments the palmar area while the feature extraction phase obtains the crease map and extracts the minutiae based on the crease map. The matching phase coarsely registers the palmprint according to a common coordinate axis and does the sector division. Sector-wise minutiae match scores are obtained and then fused to get the final match score between two palmprints.

A. *Segmentation and Contrast Enhancement*

Palmprint segmentation is challenging for the following reasons: (1) Palmar friction ridge frequency and quality change significantly over the whole palm, (2) some palmar regions may not display any friction ridge patterns, (3) inter-finger regions and regions in the middle of the palm display dark patches due to moisture in the skin (see Figure 4(a)), and (4) digits and fingers may be present in the sensed image. To overcome these problems, we have developed an algorithm utilizing Active Contour Model (ACM) to distinguish foreground and background regions. The details of the palmprint segmentation algorithm are given below:

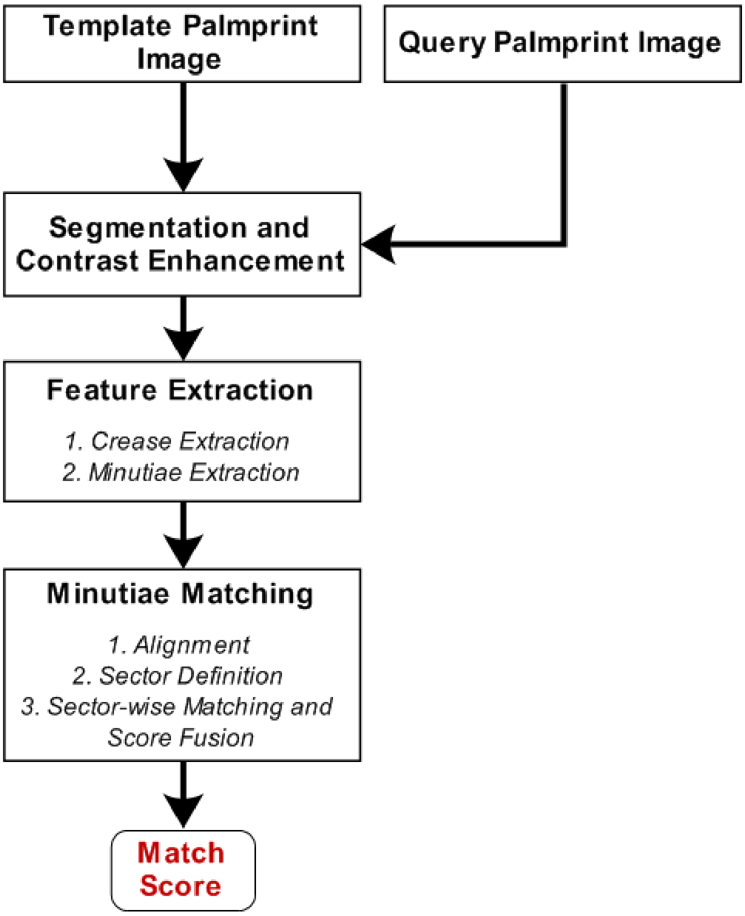

Fig. 3. Block diagram of the proposed full-to-full palmprint matching system.

- Use even-symmetric Gabor filters [14] to obtain the enhanced palmar ridge-valley structure, namely the Gabor coefficients G^* (Figure 4 (b)).
- Compute the AAD feature map from the Gabor coefficients. We divide G^* into n 8×8 non-overlapping blocks, B_i, $i = 1, 2, 3, ..., n$. The Average Absolute Deviation (AAD) for block B_i is calculated as

$$AAD(B_i) = \frac{1}{64} \sum_{(x,y) \in B_i} |G^*(x, y) - \overline{B_i}|, \tag{1}$$

where $G^*(x,y)$ is the Gabor filter coefficients for pixel (x,y), $\overline{B_i} = \frac{1}{64}\sum_{(x,y)\in B_i} G^*(x,y)$ is the mean of intensity values in B_i. High values of AAD are obtained if a ridge-valley pattern is present in block B_i.

- Since AAD features are not always able to mark the thenar palmar region, where there are very few ridge-valley structures, or the central palmar region, where the hand is not in full contact with the sensor (see Figure 4), Active Contour Model (ACM) is used [15]. This model takes the AAD feature map as input and generates the whole palm contour as the output. The active contour model can be defined as a spline minimizing a specific energy function. The fitting energy is minimized when the curve is on the desired region. The adopted ACM from [15] is based on minimizing the energy function

$$\begin{aligned} F(C,c_1,c_2) &= \mu \cdot Length(C) + \lambda_1 \int_{int(C)} |AAD(x,y) - c_1|^2 \, dx \, dy \\ &\quad + \lambda_2 \int_{out(C)} |AAD(x,y) - c_2|^2 \, dx \, dy, \end{aligned} \tag{2}$$

with respect to the contour curve C and constants c_j, $j = 1,2$; in (2) $AAD(x,y) = AAD(B_i)$ for $(x,y) \in B_i$. The parameters μ, λ_1 and λ_2 were empirically selected (equal to 1) and $int(C)$ and $out(C)$ denote, respectively, the interior and exterior regions of the closed curve C. The center and the radius of the initial curve C are set at $(170,170)$ and 50, respectively, which correspond to approximately the center of the palm and the radius such that the initial curve is completely inside the palmar region. In our experiments, the ACM converged in about 50 iterations.

After the palmprint segmentation is completed, contrast-limited adaptive histogram equalization (CLAHE) [16] is utilized to enhance the gray-scale palmprint image contrast. CLAHE is an improved version of Adaptive Histogram Equalization: It divides the palmprint image into contextual image regions and applies the histogram equalization to each region separately.

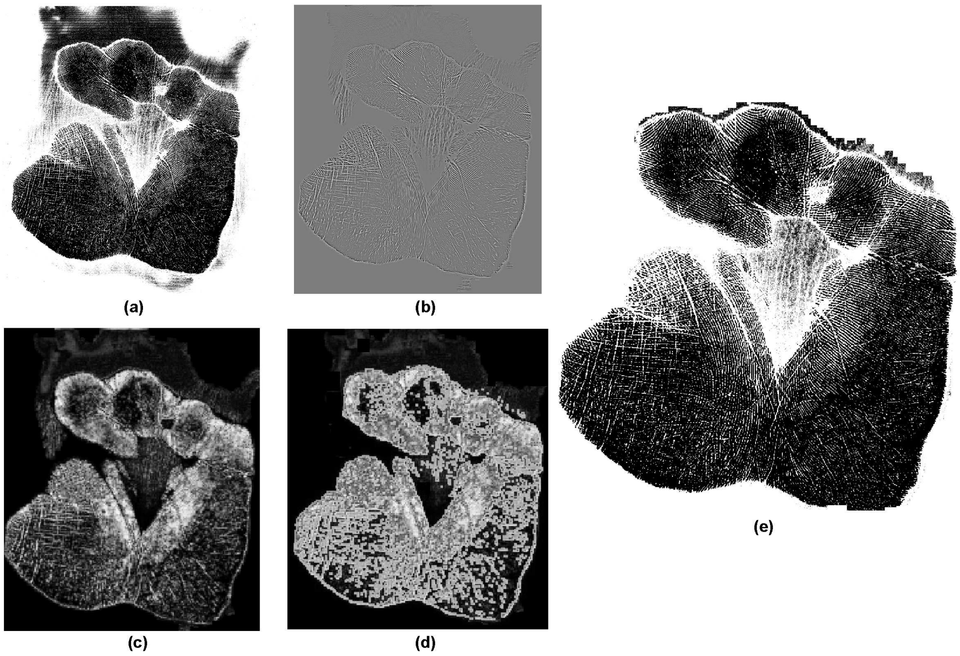

Fig. 4. Palmprint segmentation: (a) Original image, (b) Gabor coefficients, (c) AAD feature map from (b), (d) Image after ACM converged, (e) Segmented image.

B. Palmprint Feature Extraction

1) Crease Extraction: Flexion creases have a wide range of width and orientation on the same palm. Thus, we developed a multi-resolution algorithm to detect the crease regions. Three scales of palmprint images are used to detect creases with differing widths and eight directional filters are used to detect the creases with differing orientations. The details of the algorithm are given as follows:

- Since the friction ridge pattern behaves like noise for crease extraction, it is necessary to suppress the ridge-valley pattern. We adopted Gaussian smoothing with the filter width $w = 15$ and standard deviation $\sigma = 6$ to achieve this. The parameter values were decided after studying the range of inter-ridge distances on many palmprint images to get a satisfactory suppression.
- Downsampled images, I_{250} (250 ppi) and I_{125} (125 ppi), are obtained from the original image I using the nearest neighbor interpolation (see Figure 5). Downsampling any further suppresses the ridge-valley pattern.
- Directional filters [20], $g(x, y, \theta)$, with 8 different orientations are created. $g(x, y, \theta)$ is defined to be the second partial derivative of a bivariate Normal distribution with the pdf

$$\phi_2(x, y; \Sigma) = \frac{1}{2\pi \mid \Sigma \mid} e^{-\frac{1}{2}([x\,y]\Sigma^{-1}[x\,y]^T)} \tag{3}$$

with mean 0 and covariance Σ. To construct the filter with orientation θ, we rotate ϕ_2 around the origin at an angle θ resulting in $\phi_2^\theta(x, y; \Sigma) = \phi_2(x', y'; \Sigma)$. The directional filter, $g(x, y, \theta)$, with rotation θ is defined as $g(x, y, \theta) = \nabla\phi_2^\theta$. Intuitively, θ is set to {0, 22.5, 45, 67.5, 90, 112.5, 135, 157.5} (See Figure 5).
- Once I ($\equiv I_{500}$) , I_{250} and I_{125} are convolved with $g(x, y, \theta)$, we define the candidate crease regions as a set of pixels $\mathcal{S}$, where

$$\mathcal{S} = \sum_{\theta,\, n \in \{500,250,125\}} \{(x, y) :\, I_n * g(x, y, \theta)\, > \delta\}, \tag{4}$$

where δ is empirically set to -8.
- A post processing step is applied to the crease map to improve the quality. To connect the line segments close to each other in the direction of θ in each non-overlapping 60x60

block, Radon transform [21] is used. Θ is defined to be the orientation range used in Radon transform: $\Theta = \theta \pm 20^o$. The modified Radon transform that we have developed rotates the image block for each degree in Θ and checks the projection of it to see if there is a major line in any of the given directions. If there is, the pixels in that direction are connected and the final crease map is obtained as shown in Figure 5.

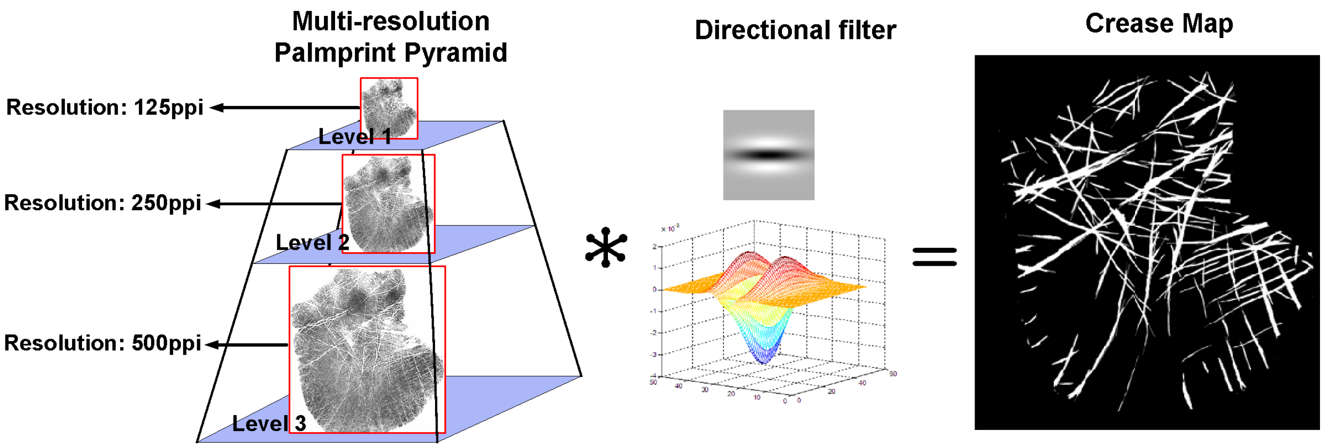

Fig. 5. Palmar crease map extraction

2) *Minutiae Extraction:* A commercial minutiae extractor and matcher, Neurotechnologija VeriFinger 4.2 [6], is used to obtain the minutiae from palmprint images. However, due to the presence of palmar creases, a large number of spurious minutiae around the palmar flexion creases are extracted. To avoid the use of the spurious minutiae in the matching phase, we utilize the palmar crease map to eliminate spurious minutiae located on the creases (see Figure 6). The average number of minutiae extracted from a full and partial palmprint image is reported in Table I.

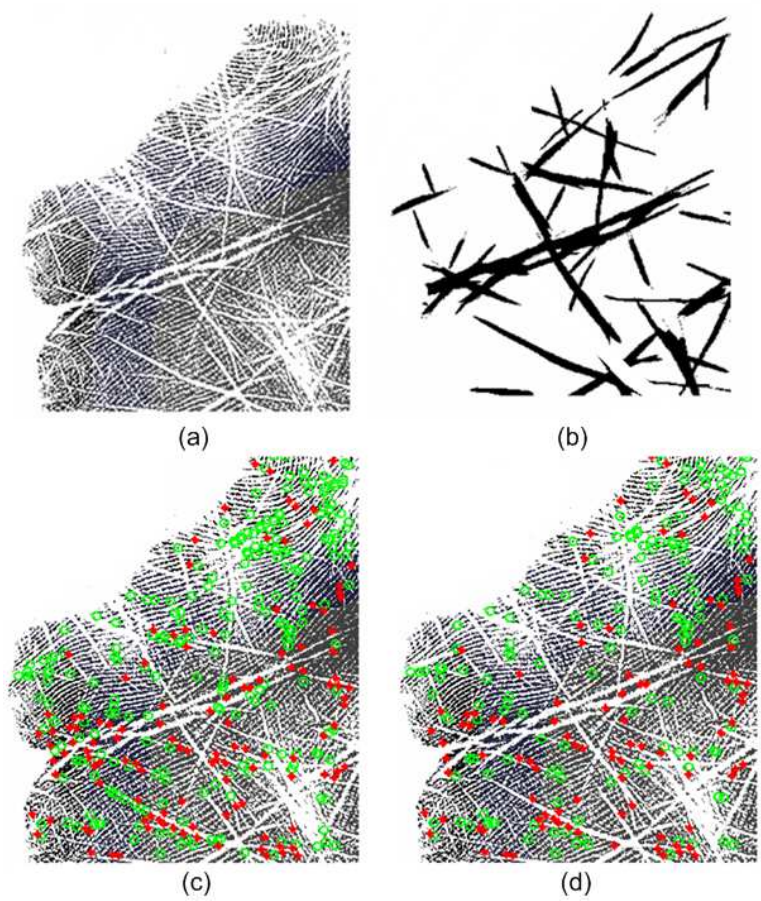

Fig. 6. Minutiae Extraction (a) A portion of palmprint image; (b) extracted creases in (a); (c) and (d) are the extracted minutiae points before and after the spurious minutiae removal procedure (red circles show the ridge endings where as the green ones show the ridge bifurcations). The number of minutiae is 364 in (c) and 260 in (d).

C. Palmprint Matching

We found it necessary to divide the segmented palmprint into sub-images since the maximum image size and minutiae feature size permitted in VeriFinger 4.2 [6], are smaller than for a typical palmprint image: maximum number of minutiae and maximum image size allowed by

TABLE I

AVERAGE NUMBER OF FEATURE POINTS OF PARTIAL AND FULL PALMPRINT IMAGES

Palmprint Image Type	# of Minutia Points Before/After Post-processing	# of SIFT Points
Full	1200/700	4,800
Synthetic Latent	106/20	500
Pseudo-Latent	115/33	2,000

VeriFinger is 1024 and 2048, respectively. However, before such an image division process, the palmprint must be aligned based on a common coordinate axis. Thus, we first align the two palmprint images and divide the palmprint images into the five sectors individually satisfying the constraints of the matcher. The matching is conducted for corresponding sectors in the two palmprint images.

1) Palmprint Alignment: The palmprint images do not contain any reliable information about the hand contour or the inter-finger regions, making it difficult to align palmprint images based on a common coordinate axis. The heart line is the most stable of the three principle lines and always starts in the same region of the palmprint (i.e. at the top of the hypothenar eminence region); we use it to coarsely align a palmprint. The details of the alignment algorithm are given for a palmprint from the left hand- the algorithm for the right hand palm follows similarly.

- To suppress the noisy ridge-valley pattern and thin creases and reduce the computational complexity, segmented palmprint image is down-sampled to a resolution of 125 ppi using the nearest neighbor approach. The upper left region of the down-sampled image is cropped with row and column sizes r_0 and c_0 given by $r_0 = r/2 - 25$ and $c_0 = c/2 + 50$, where r is the row size and c is the column size of the original image (see Figure 7(a)). In order to enhance the subimage with respect to heart line, we employ the 2D Morlet wavelet transform [19] to capture the high frequency responses where the intensity values change abruptly. The 2D Morlet wavelet is a directional wavelet that can be tuned to specific frequencies. The wavelet response

$$M(a, b, \sigma, \theta) = \frac{1}{\sqrt{\sigma}} \int\int_{R^2} I(x, y) \phi \left(\frac{x - a}{\sigma}, \frac{y - b}{\sigma}, \theta \right) dxdy \tag{5}$$

is obtained by convolution of the palmprint image $I(x, y)$ with the 2-D Morlet transform, where

$$\phi(x, y, \theta) = e^{i\, k_0\, (x\, \cos\, \theta + y\, \sin\, \theta)}\, e^{-\frac{1}{2}\sqrt{x^2 - y^2}}. \tag{6}$$

The scale factor σ is empirically set to 25, θ is the direction, k_0 is empirically set to 5.6 and (a, b) are the shifting parameters. By observing many palmprint images, we notice that the angle that heartline makes with the horizonal axis is in the range of $[-25^o, +25^o]$. Thus, we obtain the Morlet coefficients $M(a, b, \sigma, \theta)$ for 5 pre-specified values of θ, namely, $\Theta = \{-25, -12.5, 0, 12.5, 25\}$ for all the pixels (x, y) in the upper left hand region. The pixel (x, y) on the heart line provides high magnitudes of at least one of the Morlet coefficients $M(a, b, \sigma, \theta)$. We define the candidate heart line to be the set of pixels $\mathcal{S}$, where

$$\mathcal{S} = \{\, (a, b)\, :\, \prod_{\theta \in \Theta} M(a, b, \sigma, \theta)\, > \delta \}, \tag{7}$$

where δ is empirically set to 1 (see Figure 7(b)). An iterative horizontal dilation operation is applied on $\mathcal{S}$ so that the disjoint components close to each other become connected (Figure 7(c)).

- Knowing that the heart line pixels construct a line, we apply the Random Sample Consensus (RANSAC) algorithm [17] to fit a line to the point set $\mathcal{S}$, so as to distinguish the heart line pixels from the others. Once a line is fitted to the heart line pixels, two important parameters for the alignment are obtained (see Figure 7(d)): (1) The first point $P = (x_0, y_0)$ in $\mathcal{S}$ that intersects with the RANSAC line, which is assumed to be the heart line start point, and (2) the angle γ that the fitted RANSAC line makes with the horizontal axis. The existence of P is guaranteed by the dilation operations used to form connected components. Subsequently, the image is rotated around P with the angle $-\gamma$ so that the heart line aligns with the horizontal axis (Figure 7(e)).

2) Sector Division: Once the alignment is complete, we divide the image into five sectors. The five sectors numbered 1, 2, 3, 4 and 5, are defined as in Figure 8. Sectors 1 through 4 are the rectangular regions obtained by partitioning the palm by a vertical line passing through the middle of the palm and a horizontal line passing through the point $(x_0, y_0 - d_1)$, which is the point lying d_1 units vertically below the point $P = (x_0, y_0)$. Sector 5 is the square region located in the middle of the palm with opposite end points (x_1, y_1) and (x_2, y_2) given by $(x_1, y_1) \equiv (x_0 + d_3, y_0 + d_4)$ and $(x_2, y_2) \equiv (x_1 + d_2, y_1 - d_2)$, for positive numbers d_2, d_3 and d_4. In our experiments, based on the average shape of the palm, we set $d_1 = 100$, $d_2 = 1,000$, $d_3 = 100$ and $d_4 = 100$.

3) Minutiae Matching: Palmprint matching is performed by comparing the set of 2D feature points (i.e., minutiae) in a query with those in a template image. The average number of minutiae

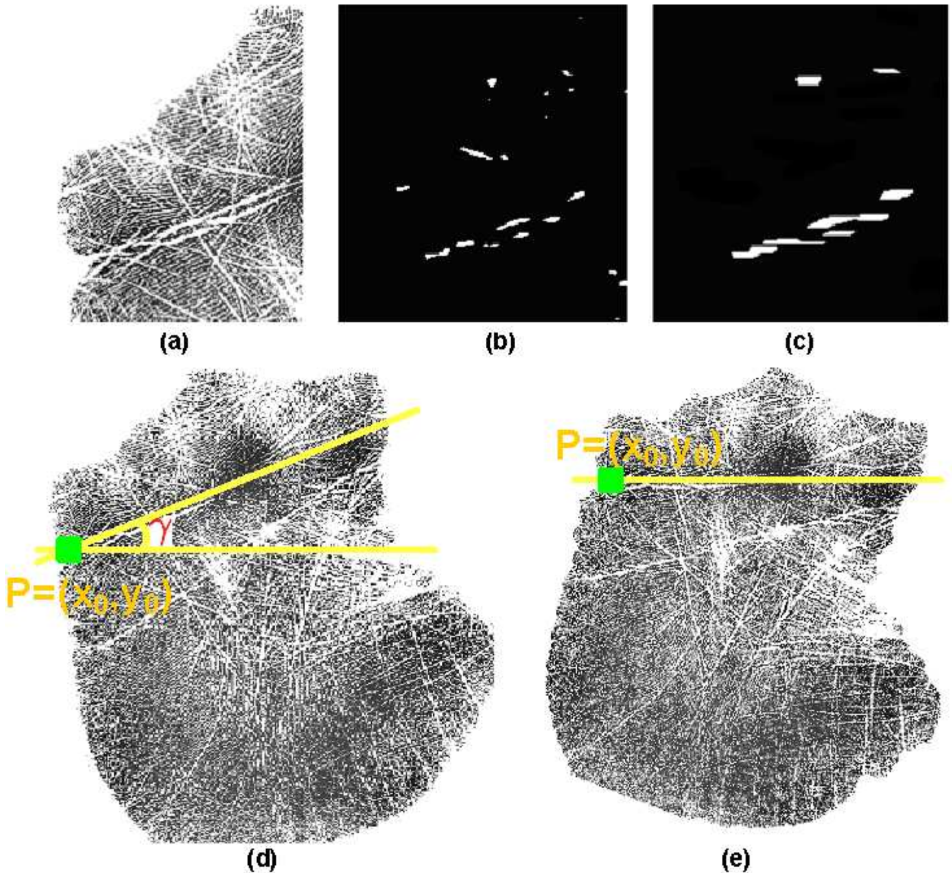

Fig. 7. Palmprint alignment procedure: (a) cropped original sub-image, (b) location of points in $\mathcal{S}$, (c) $\mathcal{S}$ after the iterative dilation and morphological operations, (d) RANSAC line fitted to $\mathcal{S}$ in (c) and angle γ, (e) the original image after alignment.

extracted from each palmprint sector is reported in Table II. For minutiae matching purpose, Neurotechnologija VeriFinger 4.2 [6], is utilized to obtain both the optimal alignment between the query and template images, and a match score.

III. Partial-to-full Palmprint Matching System

The analysis of minutiae matcher performance on partial-to-full palmprint matching shows that the minutiae matcher fails 70% of the time when the partial print does not contain reliable ridge-valley pattern. This is especially true when the partial is coming from the thenar region

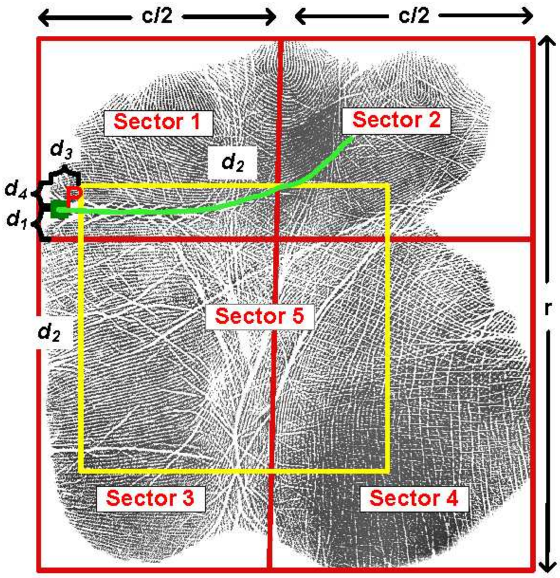

Fig. 8. Five sectors of a full palmprint image.

TABLE II

AVERAGE NUMBER OF MINUTIA POINTS IN EACH SECTOR

Sector ID	# of Minutia Points Before Post-processing	# of Minutia Points After Post-processing
Sector 1	193	103
Sector 2	195	108
Sector 3	422	233
Sector 4	417	225
Sector 5	475	242

of the palm. Since these regions contain a lot of crease (i.e. texture) information, to improve the identification performance, an additional feature set - Scale Invariant Feature Transformation (SIFT) [18] - utilizing the texture information is used in conjunction with minutiae. An example of a genuine latent-full palmprint pair, where minutiae fails, but SIFT provides high similarity score, is given in Figure 9.

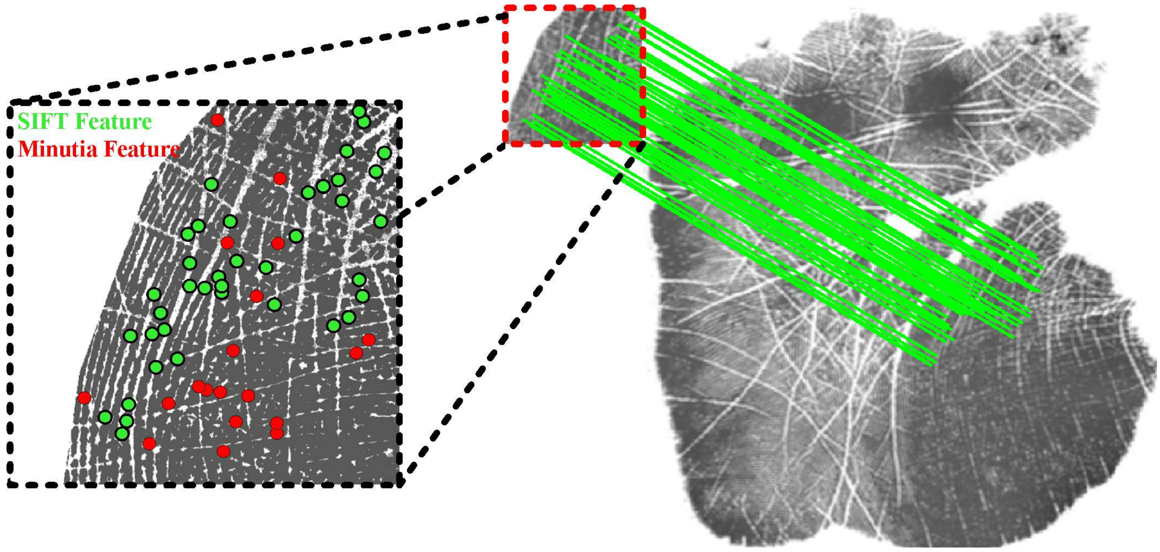

Fig. 9. A genuine pair of partial and full palmprint. The number of minutiae and SIFT features extracted from partial print are 19 and 407, respectively. Some of these points are show as red (minutiae) and green (SIFT) circles. The matching number of minutiae and SIFT features for this pair of images are 0 and 38.

The block diagram of the proposed partial-to-full palmprint matching system is shown in Figure 10. The system consists of the three major components: (1) latent ROI detection, (2) feature extraction, and (3) feature matching. Latent ROI detection phase is only applied to the full palmprint images. Since it is generally know that the latent (partial) palmprints come from specific regions of the palm (i.e. thenar, hypothenar and interdigital), these regions are automatically detected and features from these regions are utilized in the matching phase (Figure 15). The feature extraction phase obtains the crease map, SIFT feature points and extracts the minutiae based on the crease map. In the feature matching phase, minutiae and SIFT matchers are used in parallel to obtain two match scores; the score-based fusion is utilized to obtain the final match score.

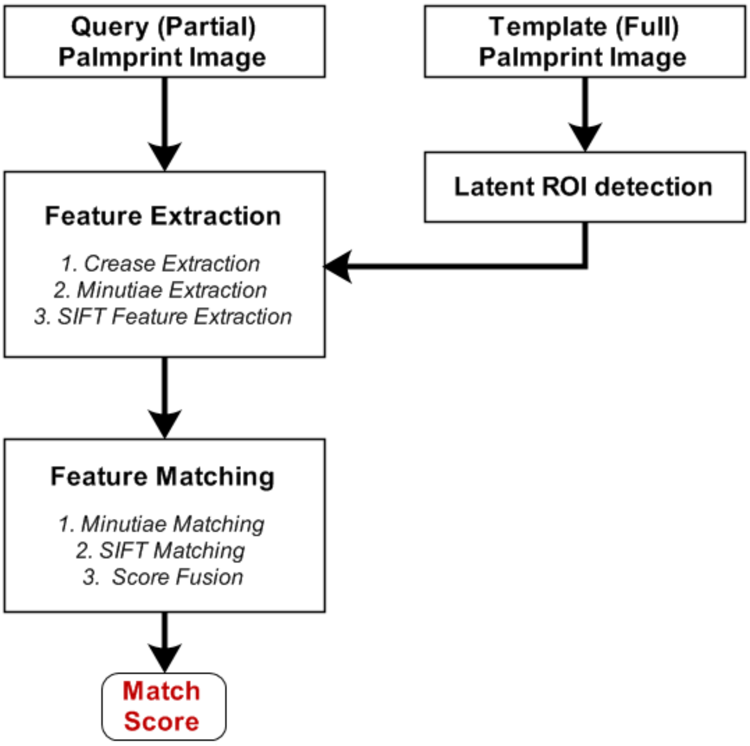

Fig. 10. Block diagram of the proposed partial-to-full palmprint matching system.

A. SIFT Feature Extraction and Matching

The SIFT algorithm extracts repeatable characteristic points, such as local extrema, from a palmprint and generates descriptors containing texture information for each feature point. The first stage of SIFT algorithm, as outlined in [18], constructs the scale space by obtaining Difference of Gaussian (DOG) images at various scales. DOG images are obtained by subtracting subsequent scales in each octave which is a set of successive down sampled and Gaussian-smoothed original image. Subsequently, local extrema points are found by searching for stable features in the DOG space across different scales. In order to detect the local extrema points, each pixel is compared with their neighboring pixels in the DOG images and the ones with smallest (or, largest) values are selected as the local extrema points. Detected extrema points which lie on an edge (or, unstable) are removed since these points cannot be detected again for different viewpoints or lighting levels. For each feature point, a descriptor is obtained by using the histogram of gradient orientation around the corresponding local extremum (4x4 array of histograms with 8 different orientation bins in each). Moreover, the gradient orientation is rotated with respect to the dominant orientation of each local extremum to make the descriptor orientation invariant. In our experiments, we utilized the SIFT implementation by Lowe in [18], where the parameters, number of octaves, number of scale samples per octave are set to 5 and 3, respectively. In Figure 11, extracted SIFT points from a full and synthetic latent palmprint and their matching result are shown. The average number of SIFT feature points extracted from a full and partial palmprint image is reported in Table I.

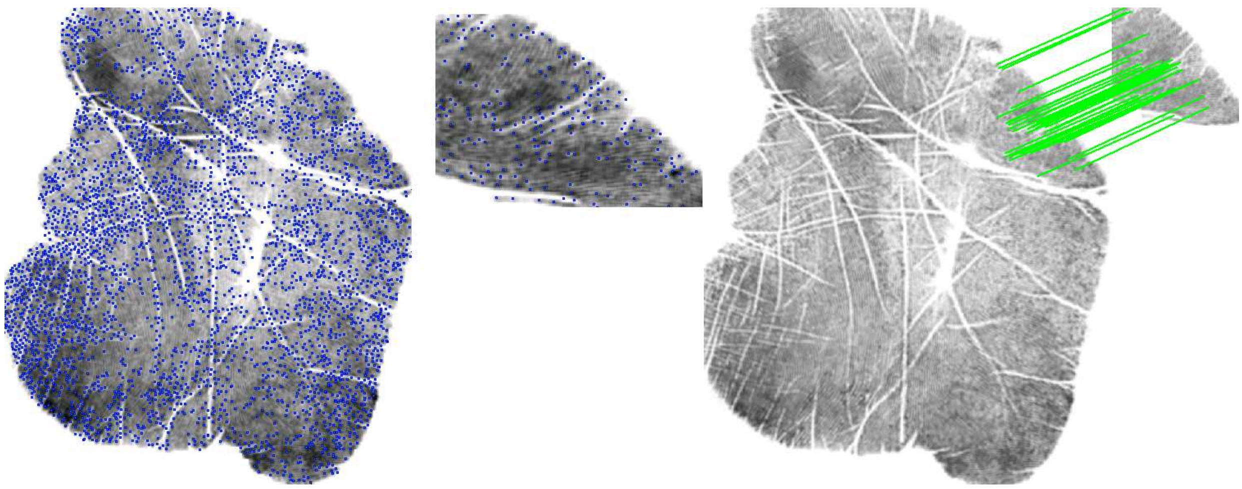

(a) (b)

Fig. 11. Detecting SIFT features from palmprint: (a) SIFT feature points extracted from a pair of genuine (full and synthetic partial) images, and (b) SIFT matching result for a genuine pair. The matching score is 50.

SIFT's point-wise matching is achieved by identifying the top 2 closest points to a key point based on Euclidean distance between associated descriptors. Matching measure is obtained by comparing the distance of the closest neighbor ($d1$) to that of the second-closest neighbor ($d2$). When $d1/d2$ is sufficiently small, the key point matches its closest point. In our experiments, the ratio values is set to 0.75. Moreover, the matching score between two images is defined to be the number of matching points (See Figure 11).

IV. EXPERIMENTAL RESULTS

A. 500 ppi Palmprint Database

Full Palmprint Database: To our knowledge, there is no 500 ppi resolution palmprint database publicly available. Thus, we collected a 500 ppi palmprint database from 100 unique palms (50 subjects x 2 palms per subject) using a Cross Match LSCAN 1000P sensor. Each palm contributed 10 impressions (5 impressions x 2 sessions with an interval of seven days) resulting in 1,000 palmprint images.

Partial Palmprint Database: We created a synthetic latent palmprint database (Figure 12 (b)) from 100 unique palms (50 subjects x 2 palms per subject x 5 partial print per palm). As it is shown in Figure 12 (a), latent palmprint images mostly come from the thenar, hypothenar and interdigital regions of the palm. In order to simulate this, we developed a model defining palmar ROI. The center location of a synthetic latent palmprint is randomly selected from the ROI, and a 500×500 sub-image containing at least 70% of the palmar region is cropped from the full palmprint image. Figure 12 (b) gives examples of a simulated partial print. This procedure is also applied to the full palmprint images which are compared to partial palmprint images based on minutiae features. The reason for this is to remove the minutiae in the mid-region of the palmprint and also to be able to meet the constraints of the Neurotechnologija VeriFinger 4.2 [6] minutiae matcher.

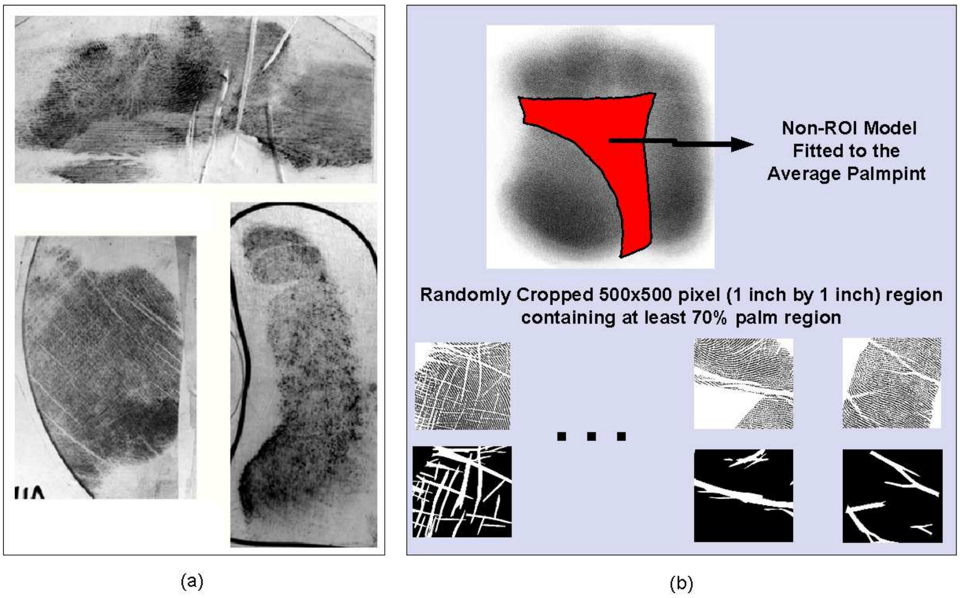

Fig. 12. (a) Latent palmprint images from most commonly seen parts of palm, (b) Synthetic latent palmprint generation.

B. Experimental Results

1. Full-to-full palmprint matching. Each full palmprint in our database was matched with every other palmprint. This resulted in 4,500 genuine and 24,500 impostor matches. Once the the minutiae matching results are obtained for each sector, we get the full-to-full palmprint matching score using sum-rule based score-level fusion (Figure 13). Sector-wise matching shows the amount of friction ridge information present in each sector. Since the minutiae information in Sector 4 (thenar region) is not very reliable, it is the worst performing sector for minutiae matcher. On the other hand, Sector 5 is one of the best sectors since it is rich in reliable crease and minutiae information.

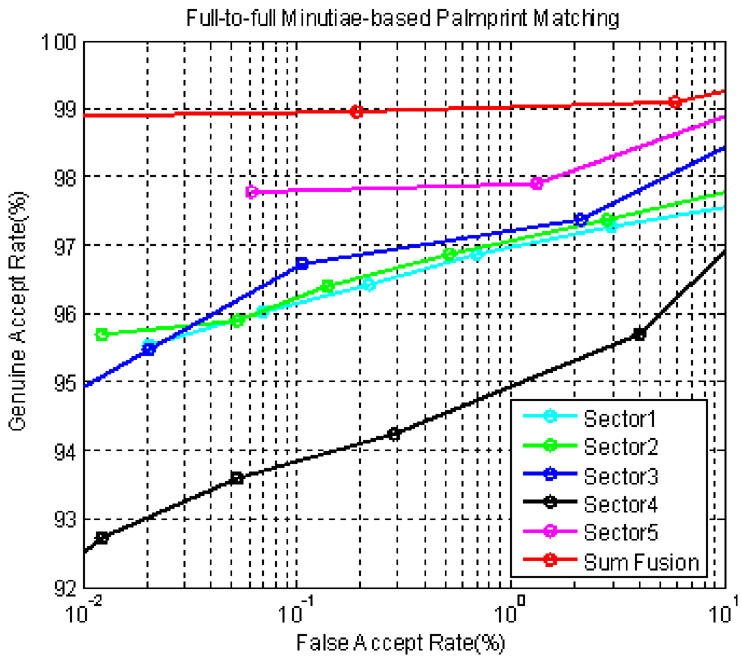

Fig. 13. ROC curves for full-to-full palmprint matching based on minutiae

2. Partial-to-full palmprint matching. We obtained the retrieval performance for 500 randomly cropped synthetic latent palmprint; 50,000 comparisons are carried out based on 500 partial and 100 full palmprint images. As shown in Figure 14, SIFT feature based matching provides much better identification rate : $\sim 91\%$ compared to the minutiae matcher's $\sim 82\%$ identification rate for rank-1 retrieval. A combination of minutiae and SIFT match scores gives even a higher identification rate. We adopted min-max normalized weighted sum-rule based fusion, where 0.8 and 0.2 are the chosen weights for SIFT and minutiae matchers, respectively. Consequently, the partial palmprint identification achieves $\sim 96\%$ rank-1 matching accuracy.

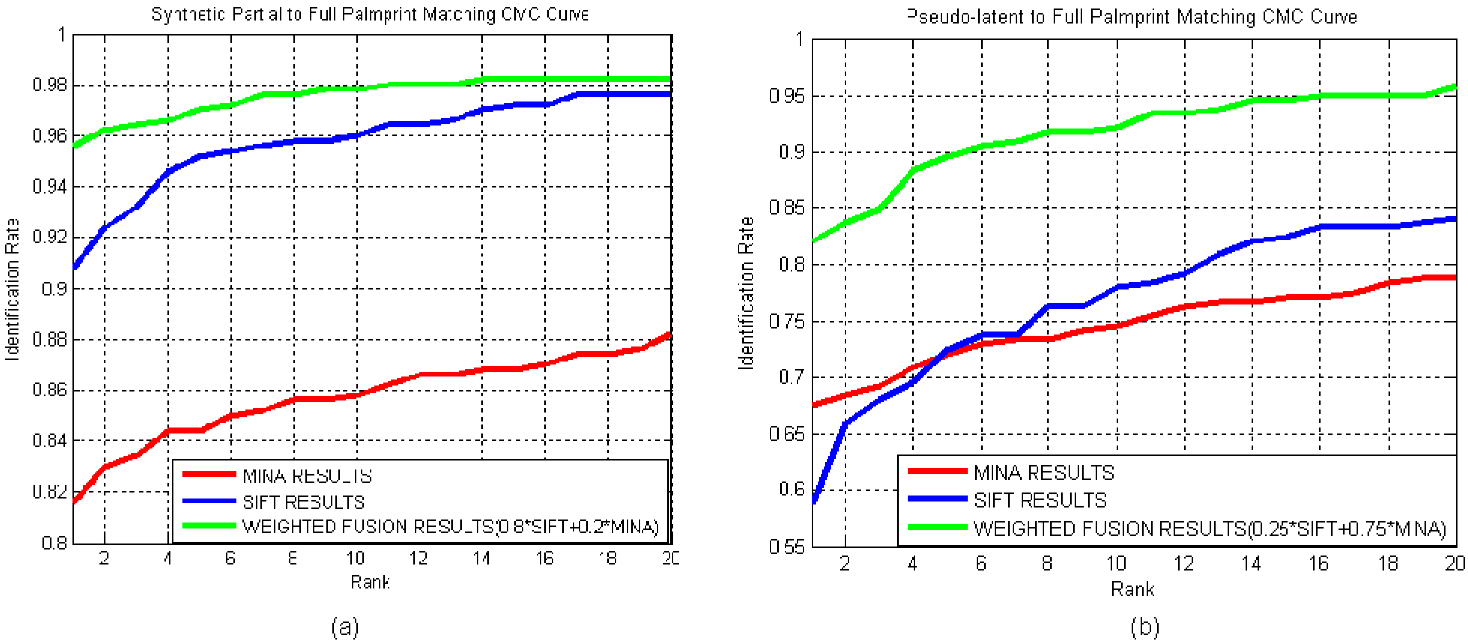

Fig. 14. CMC curves for (a) synthetic latent-to-full and (b) pseudo latent-to-full palmprint matching using minutiae and SIFT features

We repeated the partial-to-full matching experiment also on the pseudo-latent database (Figure 15) that we collected from 20 unique palms, 240 images (10 subjects x 2 palms per subject x 12 partial print per palm). Compared to the performance from synthetic latent experiment, the performance of SIFT and minutiae matcher drops dramatically (i.e. approximately 30% and 14%, respectively) for pseudo-latent experiment. Weighted sum-rule based score-level fusion is again utilized with a weight of 0.75 for minutiae matcher and 0.25 for SIFT matcher, leading an increase in the fusion performance to 82% compared to 96% for the syntectic partial performance. The reason for such a drop in performance is due to the fact that the pseudo-latent database images (see Figure 15) collected are not as of high quality as the ones cropped from the full palmprint images and non-linear deformation is introduced by the subject while placing the certain region of the palm on platen. We also observed that the overlapping area between the full and partial palmprint can be the dominating factor for not being able to get a good matching score for a genuine pair; for instance, partial print created by the hypothenar eminence region of the palm, also called writes's palm, may not have a significant overlapping area with the corresponding full palmprint in the system. It should be noted that these are the cases also observed with the actual latent palmprint images lifted from crime scenes.

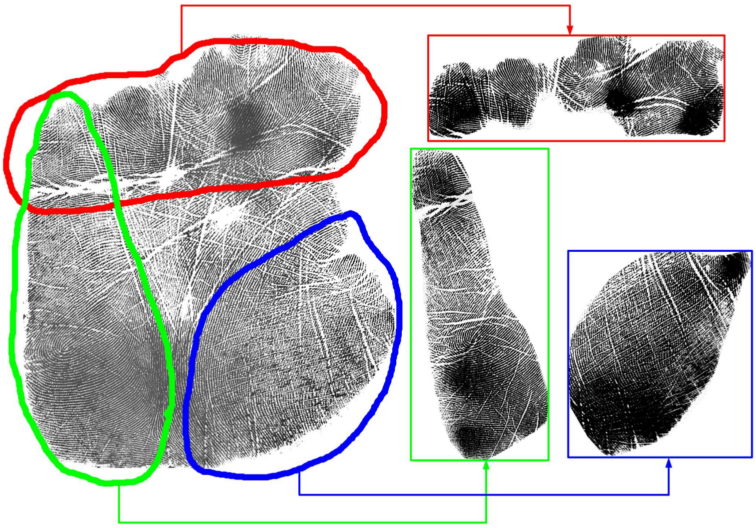

Fig. 15. A pair of full and pseudo-latent palmprint images.

The average time taken for palmprint preprocessing (segmentation, alignment and sector division), feature extraction (crease-map, minutiae and SIFT), matching of minutiae and SIFT feature points are 25 seconds per image, 15 seconds per image and 5 seconds per match, respectively, when tested on a PC with 2 GB of RAM and a 2.13 GHz Intel Core 2 CPU.

V. Summary and Conclusion

Since the commercial applications utilize features from low resolution images, they cannot be adopted for forensic applications; thus, we have developed a palmprint matching system utilizing different 500 ppi palmar features, namely friction ridges, minutiae, flexion creases and palmar texture. Our system can match either a full or latent input image to a database of full palmprint images. Our algorithm utilize Gabor filters and Active Contour Model for palmprint segmentation. Palmar creases with different widths and orientations are detected by using a palmprint image pyramid approach with directional filters. Further, we have proposed a new feature set to improve the accuracy of the system: the palmar texture is represented by the local extrema points obtained by SIFT algorithm. Since there is no public domain 500 ppi palmprint database, the experiments are conducted on a 500 ppi palmprint image database collected in our lab. We have shown that the 500 ppi palmar features provide high performance in the case of full-to-full palmprint matching. In case of partial-to-full palmprint matching, we have obtained the experimental results both on synthetic latent and pseudo-latent palmprint databases. We have observed that score-based fusion of minutiae and SIFT feature matching provides a better retrieval performance compared to the individual matchings. Currently, we are in the process of improving our algorithm and acquiring a larger database for testing it. We are also investigating palmar Level 3 features which can be used in the case of 1000 ppi partial-to-full palmprint matching.

References

[1] *http://www.businesswire.com,* El Paso police installs Sagem Morpho Palmprint System, Business Wire, 2002.

[2] S. K. Dewan, W. Elementary, “Scan a Palm, Find a Clue”, The New York Times, November 2003.

[3] *http://www.biometrics.gov/Documents/BioHistory.pdf*,Biometrics History, 2007.

[4] *http://www.ibia.org/membersadmin/casestudy/pdf/20/Australia%20CrimTrac%2012-08-04.pdf*, Australian NAFIS replacement and palmprint upgrade project, 2004.

[5] ANSI/NIST-ITL 1-2000, "Data Format for the Interchange of Fingerprint, Facial and SMT Information," ftp://sequoyah.nist.gov/pub/nist internal reports/sp500-245-a16.pdf.

[6] "Neurotechnologija Verifinger 4.2 SDK," http://www.neurotechnologija.com/vfsdk.html.

[7] F. Galton, *Fingerprints* (reprint), Da Capo Press, New York, 1965.

[8] D. R. Ashbaugh, *Quantitative-Qualitative Friction Ridge Analysis: An Introduction to Basic and Advanced Ridgeology*, *CRC Press*, 1999.

[9] N. Duta, A.K. Jain, and K.V. Mardia,"Matching of Palmprint," Pattern Recognition Letters, vol. 23, no. 4, pp. 477-485, 2001.

[10] D. Zhang, A.W. Kong, J. You and M. Wong, "Online Palmprint Identification," IEEE Trans. Pattern Anal. Mach. Intell., vol. 25, No. 9, pp. 1041-1050, Sept. 2003.

[11] Z. Sun, T. Tan, Y. Wang, and S.Z. Li, "Ordinal Palmprint Representation for Personal Identification," Conference on Computer Vision and Pattern Recognition (CVPR),vol. 1, pp. 279-284, Jun. 2005.

[12] H. Cummins and M. Midlo, "Finger Prints, Palms and Soles: An Introduction To Dermatoglyphics," Dover Publications, New York, 1961.

[13] Peter Komarinski, *Automated Fingerprint Identification Systems*, Academic Press, 2004.

[14] L. Hong, Y. Wan, and A.K. Jain,"Fingerprint Image Enhancement: Algorithms and Performance Evaluation," IEEE Trans. Pattern Analysis and Machine Intelligence, vol. 20, no. 8, pp. 777-789, Aug. 1998.

[15] T. Chan and L. Vese, "Active Contours without Edges," IEEE Trans. Image Processing, vol. 10, no. 2, pp. 266-277, 2001.

[16] S. M. Pizer, E. P. Amburn, J. D. Austin, R. Cromartie, A. Geselowitz, T. Greer, B. M. ter Haar Romeny, J. B. Zimmerman, and K. Zuiderveld, "Adaptive Histogram Equalization and its Variations," Computer Vision, Graphics and Image Processing, vol. 39, pp. 355-368, 1987.

[17] M. A. Fischler, R. C. Bolles., "Random Sample Consensus: A Paradigm for Model Fitting with Applications to Image Analysis and Automated Cartography," Comm. of the ACM, vol. 24, pp. 381-395, 1981.

[18] D. Lowe, "Distinctive Image Features from Scale-invariant Key Points," International Journal of Computer

Vision, vol. 60, pp. 91-110, 2004.

[19] Burrus, C. and Gopinath, R. and Guo, H., *Introduction to Wavelets and Wavelet Transforms*. Prentice Hall, 1998.

[20] T. Leung and J. Malik, "Representing and recognizing the visual appearance of materials using 3D textons," International Journal of Computer Vision , vol. 43, no. 1, pp. 29-44, 2001.

[21] R. N. Bracewell, *Two-Dimensional Imaging*. Prentice Hall, 1995.